arXiv:astro-ph/0310347v2 20 Nov 2003

GBT DISCOVERY OF TWO BINARY MILLISECOND PULSARS IN THE GLOBULAR CLUSTER M30

SCOTT M. RANSOM[1,2], INGRID H. STAIRS[3], DONALD C. BACKER[4], LINCOLN J. GREENHILL[5], CEES G. BASSA[6],
JASON W. T. HESSELS[1], VICTORIA M. KASPI[1,2,7]
Submitted to ApJ

ABSTRACT

We report the discovery of two binary millisecond pulsars in the core-collapsed globular cluster M30 using the Green Bank Telescope (GBT) at 20 cm. PSR J2140−2310A (M30A) is an eclipsing 11-ms pulsar in a 4-hr circular orbit and PSR J2140−23B (M30B) is a 13-ms pulsar in an as yet undetermined but most likely highly eccentric ($e > 0.5$) and relativistic orbit. Timing observations of M30A with a 20-month baseline have provided precise determinations of the pulsar's position (within $4''$ of the optical centroid of the cluster), and spin and orbital parameters, which constrain the mass of the companion star to be $m_2 \gtrsim 0.1\,M_\odot$. The position of M30A is coincident with a possible thermal X-ray point source found in archival *Chandra* data which is most likely due to emission from hot polar caps on the neutron star. In addition, there is a faint ($V_{555} \sim 23.8$) star visible in archival *HST* F555W data that may be the companion to the pulsar. Eclipses of the pulsed radio emission from M30A by the ionized wind from the compact companion star show a frequency dependent duration ($\propto \nu^{-\alpha}$ with $\alpha \sim 0.4$–0.5) and delay the pulse arrival times near eclipse ingress and egress by up to 2–3 ms. Future observations of M30 may allow both the measurement of post-Keplerian orbital parameters from M30B and the detection of new pulsars due to the effects of strong diffractive scintillation.

Subject headings: galaxy: globular clusters: individual: M30 — pulsars: individual: PSR J2140−2310A — radio continuum: stars

1. INTRODUCTION

Globular clusters (GCs) produce millisecond pulsars (MSPs) at a rate per unit mass that is up to an order-of-magnitude greater than the Galaxy(e.g. Kulkarni & Anderson 1996). Due to the relatively large distances of GCs (several to tens of kiloparsecs), the low intrinsic luminosities of MSPs, and the fact that most MSPs are members of compact binary systems, the discovery of new cluster pulsars requires long observations with the largest radio telescopes and computationally intensive data analysis.

The discovery of new cluster pulsars is interesting because of the wide variety of science that can result from using them as sensitive probes into the natures of the pulsars themselves and the clusters in which they live. Recently, cluster pulsars have been used to probe properties of GCs, such as the mass-to-light ratios in cluster cores (e.g. Freire et al. 2001a; D'Amico et al. 2002), cluster proper motion (Freire et al. 2003), and the ionized gas content in 47 Tucanae (Freire et al. 2001b). For binary pulsars, timing observations have measured relativistic effects such as the advance of periastron (and therefore the total mass) in the 47 Tuc H system (Freire et al. 2003), and probed the companion winds and eclipse mechanisms for several known eclipsing MSPs (e.g. D'Amico et al. 2001b; Possenti et al. 2003). The precise astrometry provided by MSP timing has allowed the op-

tical identification of several binary MSP companions (e.g. Ferraro et al. 2001; Edmonds et al. 2002), which is crucial for determining the nature of the companion stars, and the X-ray identification of many MSP systems (e.g. Grindlay et al. 2002), which gives us useful information on pulsar emission and neutron star cooling mechanisms. Finally, many theorists have predicted that truly exotic pulsar systems, such as a pulsar-black hole binary (e.g. Sigurdsson 2003), will be found in GCs.

After a flurry of GC pulsar discoveries in the 1980s and early 1990s, the number of known cluster pulsars remained virtually constant ($\sim$35) until 2000 (for a review, see Kulkarni & Anderson 1996). Over the past several years, however, the art of searching for radio pulsars in GCs has undergone a renaissance due to the development of very sensitive (i.e. low-noise and high-bandwidth) 20-cm receivers (e.g. Staveley-Smith et al. 1996) and the increasing availability of the high performance computing resources required to conduct sensitive but specialized searches for binary millisecond pulsars in observations with durations of several hours (e.g. Johnston & Kulkarni 1991; Ransom, Eikenberry, & Middleditch 2002). The Parkes radio telescope has been particularly productive as of late with the discovery of at least 24 millisecond pulsars in 8 GCs, most of which are in binaries (Camilo et al. 2000; D'Amico et al. 2001a,b; Possenti et al. 2001; Ransom 2001; D'Amico et al. 2002; Lorimer et al. 2003; Possenti et al. 2003).

In the past two years, the recently upgraded Arecibo telescope and the new 100-m Green Bank Telescope (GBT) have become available, and several new algorithms have been developed to improve search sensitivities to binary MSPs in compact orbits (Chandler 2003; Ransom, Cordes, & Eikenberry 2003). Using the GBT and one of these new techniques, Jacoby et al. (2002) have recently reported the discovery of three new binary MSPs in M62 (see also Chandler 2003). With these advances in mind, we undertook a major survey of rich and/or nearby GCs at

[1] McGill University Physics Dept., Montreal, QC H3A 2T8, Canada; ransom@physics.mcgill.ca
[2] Center for Space Research, Massachusetts Institute of Technology, Cambridge, MA 02139
[3] Dept. of Physics and Astronomy, University of British Columbia, 6224 Agricultural Road, Vancouver, BC V6T 1Z1, Canada
[4] Dept. of Astronomy and Radio Astronomy Laboratory, University of California at Berkeley, 601 Campbell Hall 3411, Berkeley, CA 94720
[5] Harvard-Smithsonian Center for Astrophysics, 60 Garden St., Cambridge, MA 02138
[6] Astronomical Institute, Utrecht University, PO Box 80 000, 3508 TA Utrecht, The Netherlands
[7] Canada Research Chair, Steacie Fellow, CIAR Fellow

20 cm that are visible from Arecibo and/or the GBT. We are analyzing the data using modern search algorithms and techniques. This is the first in a series of papers describing the results from these observations. Specifically, we focus on "First Science" data from the GBT, taken in the Fall of 2001 toward 12 GCs. Additional discoveries — including at least one other new MSP in M13 discovered in the GBT data described below — and results from the rest of the project will be presented elsewhere[8].

2. SEARCH OBSERVATIONS AND DATA ANALYSIS

In 2001 September and October, we used the Gregorian focus 20-cm receiver (1.15−1.73 GHz usable bandwidth with $T_{sys} \sim 25$ K) on the GBT to observe 12 different clusters for either 4 hrs (M2, M4, M75, M80, M92, and NGC 6342) or 8 hrs (M3, M13, M15, M30, M79, and Pal1) each. Since the GBT beam has a FWHM of nearly 9′ at 20 cm, single pointings fully covered each cluster. Samples from two orthogonal polarizations were transmitted through fiber optic cables to the observatory control room where they were fed to either one or two Berkeley-Caltech Pulsar Machines[9] (BCPMs; Backer et al. 1997). The BCPMs are analog/digital filterbanks which 4-bit sample each of 2×96 channels at flexible sampling rates and channel bandwidths and which can sum the two polarizations in hardware if requested.

We observed each cluster using 96×1.4 MHz channels of 2 summed polarizations centered at 1375 MHz and sampled every 50 μs. For those observations using a second BCPM (which included the observations of M30), we recorded 96×1.0 MHz channels with summed polarizations sampled every 36 μs at a center frequency of 1490 MHz. In total, these initial search observations generated ∼0.5 TB of data, which were stored on DLT IV magnetic tapes.

Reduction of the data took place on a dedicated Beowulf-style cluster of 52 dual-processor 1.4 GHz AMD Athlon workstations located at McGill University. The available computing power allowed us to attempt extensive interference removal (see below) and to conduct fully coherent acceleration searches[10] for binary pulsars in all clusters. In previous GC pulsar projects acceleration searches were only used on clusters where pulsars — and therefore the dispersion measure (DM) to the cluster — were known *a priori*, due to the computational expense of searching over the additional "acceleration" parameter.

Since these data were taken as part of the GBT "First Science" program, the telescope was still in the early stages of commissioning and the radio frequency interference (RFI) environment was quite bad. Each of the observations contained large quantities of both persistent and transient broadband and narrowband interference. The very strong Lynchburg, Virginia airport radar, with a rotational period of approximately 12 s, was particularly destructive and effectively eliminated any sensitivity we should have had to weak pulsars with periods longer than ∼ 100 ms. Due to the challenges involved in excising this RFI, approximately one quarter of these data remain to be fully analyzed.

We searched the raw data from each cluster for RFI in both the time and frequency domains as a function of both BCPM channel and time (in units of ∼10 s). Sections of data containing fluctuations significant at the 4-σ level in the frequency domain or 10-σ level in the time domain were masked using the running median of the appropriate BCPM channel. In addition, we computed and Fourier transformed non-dispersed topocentric time series in order to identify strong and obvious terrestrial interference (i.e. occurring at "un-natural" frequencies such as 11.1̄ Hz) which we ignored in subsequent stages of the analysis.

After applying the interference masks, we de-dispersed the data over a range of DMs from ∼50−200% of the predicted DM of the cluster (using the galactic electron density model of Taylor & Cordes 1993), or, for clusters with known pulsars, from ∼90−110% of the average DM of those pulsars. The clusters that we observed with the GBT were chosen partly because their known or predicted DMs were ≲100 pc cm^{-3}, thereby keeping the dispersive smearing across each BCPM channel to ≲0.5 ms at 20 cm. The stepsize in DM was chosen to produce no more than ∼0.2−0.3 ms of dispersive smearing across the 134.4 MHz bandwidth. The final stage of data preparation involved removing samples from or adding samples to the time series as appropriate in order to account for the observatory's motion with respect to the solar system barycenter (using the DE200 ephemeris of Standish 1982).

After Fourier transforming each de-dispersed and barycentered time series and removing the previously identified RFI signals and their harmonics, we searched the data for pulsations in three steps: 1) using acceleration searches of the full-length observation to maximize our sensitivity to isolated or long-period binary pulsars, 2) with acceleration searches of overlapping ∼20 min and ∼60 min segments of the observation to improve our sensitivity to pulsars in compact binaries or which exhibit significant diffractive scintillation, and 3) using phase-modulation (or sideband) searches for pulsars in ultra-compact ($P_{orb} \lesssim 2$ hr) binary systems (Ransom et al. 2003). For the acceleration searches, we used a modern Fourier-domain matched-filtering code that includes Fourier interpolation and the incoherent harmonic summing of the first 1, 2, 4, and 8 harmonics of any potential signal (Ransom 2001). The acceleration search code allowed the highest summed harmonic to linearly drift by up to 170 Fourier frequency bins during the portion of the observation being searched (lower harmonics drift a smaller fraction of bins equal to their harmonic number over that of the the highest harmonic). We folded the raw data for interesting acceleration search candidates over a range of nearby periods, period derivatives, and DMs in order to maximize the signal-to-noise ratio. For phase-modulation candidates, we used Fourier-domain matched-filtering of orbital templates as described in Ransom et al. (2003).

Given the highly variable RFI environment, the often extreme effects of diffractive scintillation (see §4.2), and the sensitivity losses caused by uncorrected orbital motion for binary pulsars, it is difficult to place a hard limit on our overall search sensitivity. However, based on search simulations, our detections of known cluster pulsars, and the radiometer equation, we estimate that we were sensitive to "normal" millisecond pulsars with flux densities in the range ∼50−100 μJy. Our sensitivities to sub-millisecond pulsars and ultra-compact binary MSPs are factors of ∼2−3 worse than the above values due primarily to the effects of dispersive smearing across the relatively wide BCPM channels for the former and the incoherent nature of the phase-modulation search technique for the latter. For slow pulsars ($P \gtrsim 0.1$ s), our sensitivities were

---

[8] An up-to-date catalog of GC pulsars can be found at http://www.naic.edu/$\sim$pfreire/GCpsr.html

[9] http://www.gb.nrao.edu/$\sim$dbacker

[10] Acceleration searches correct either a time series or its Fourier transform to account for large apparent period derivatives in the signals from binary pulsars in compact orbits (see e.g. Johnston & Kulkarni 1991).
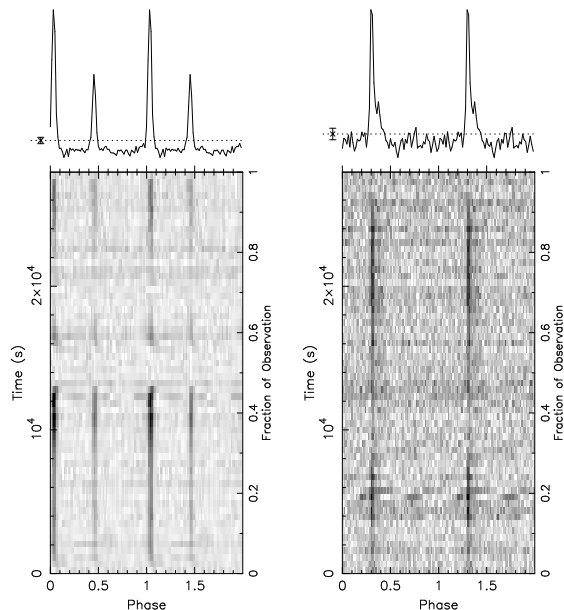
FIG. 1.— Pulse profiles from the 7.8-hr discovery observation of the 11-ms binary pulsar PSR J2140−2310A (M30A, left) and the 13-ms eccentric binary pulsar M30B (right). The Doppler effects of each orbit have been removed, and two complete profiles are plotted for clarity. The data were taken with the GBT on 2001 September 9 using the BCPM1 machine (see §2) at a center frequency of 1370 MHz with an effective time resolution of ∼0.12 ms. The greyscale below the average pulse profiles shows the consistency of the pulsed emission as well as some effects due to interference as a function of time. Strong scintillation and portions of at least two eclipses of M30A are evident, including dispersive delays to the pulse arrival times at eclipse ingress and egress (see §4.3).

degraded even more due to the devastating effects of RFI, and in particular, the Lynchburg radar.

3. DISCOVERIES AND TIMING OBSERVATIONS

One of the most promising clusters in our search was M30 (NGC 7099; $l = 27°.18$, $b = −46°.84$), due its "post-core-collapsed" nature and relatively high central luminosity density. M30 has a measured core of $<2.5''$ as determined by *HST* (Yanny et al. 1994), and an age and distance of 12.3 Gyr and $D = 9.0 ± 0.5$ kpc (apparent distance modulus $m_v − M_v = 14.90 ± 0.05$, $E(B−V) = 0.039$; Carretta et al. 2000) respectively as determined from *Hipparcos* data. Significant evidence has been found of mass segregation within the cluster (Guhathakurta et al. 1998).

While performing acceleration searches of ∼20 min segments of BCPM1 data for M30 taken 2001 September 9, we discovered two highly variable and highly accelerating pulsar candidates near 11 ms (M30A; see §4) and 13 ms (M30B; see §5), whose signal-to-noise ratios peaked at DMs very near 25 pc cm⁻³. Upon examining the BCPM2 data from the same time period, we confirmed both of these candidates as pulsars with very high significance. Soon thereafter, we determined "local" timing solutions for these data consisting of a compact 4.2-hr orbit for M30A and a high-order polynomial expansion in spin frequency for M30B which showed each pulsar visible for ∼90% of the 7.8 hr observation (see Fig. 1).

Our discovery of two MSPs within the 9′ beam of the GBT at 20 cm — at least one of which is within 4″ of the cluster center ($\alpha_{M30} = 21^h 40^m 22^s.16 ± 0''.2$, $\delta_{M30} = −23° 10' 47''.6 ± 0''.2$; J2000; see §4.4) — and which have measured DMs (∼25 pc cm⁻³) similar to that predicted for the cluster using both the Taylor & Cordes (∼23 pc cm⁻³; 1993) and the

NE2001 (∼41 pc cm⁻³; Cordes & Lazio 2002) models of the galactic electron density, firmly establish these as the first known pulsar members of M30.

In 2002 March, we began a series of monthly 4−8 hr observations of M30 using the GBT/BCPM1 setup described in §2. We have been unable to use the second BCPM machine during these sessions due to problems with the instrument. The observations were intended to establish phase coherent timing solutions for both pulsars and to allow us to search for new pulsars in M30 whose measured flux densities were temporarily boosted above our detection limits via scintillation. On several occasions, we observed M30 with 48 MHz of bandwidth centered at either 575 MHz or 820 MHz in order to determine the DM of the pulsars more accurately, take advantage of a better RFI environment (particularly for 820 MHz), and to search for pulsars with spectral indices too steep to be detected near 1400 MHz.

4. PULSAR J2140−2310A (M30A)

For pulsar M30A we folded the raw data from the timing observations modulo the predicted pulse period given our best orbital ephemeris and accumulated the resulting pulse profile until enough signal was available to allow an accurate measurement of the phase of the pulsation. We measured the pulse phase by cross-correlating (in the Fourier domain; Taylor 1992) the observed profiles with a high signal-to-noise template profile determined during a period of scintillation-heightened flux density. Absolute times-of-arrival (TOAs) resulted by referencing the phase measurement to the start time of each observation as recorded from the observatory clock. We later used TEMPO[11] to correct these times to the UTC(NIST) time standard with data from the Global Positioning System and to transform them to the solar-system barycenter using the DE200 planetary ephemeris (Standish 1982).

Using TEMPO, we then fit the TOAs iteratively to a model incorporating the pulsar position, DM, spin period (P), period derivative ($\dot{P}$), and the Keplerian orbital parameters for a circular orbit; the projected semi-major axis ($x \equiv a \sin i/c$), the orbital period (P_{orb}), and the time of the ascending node (T_{asc}). Attempts to fit for eccentricity resulted in a 95% confidence upper limit of $e < 1.2 × 10^{-4}$. The timing model produced RMS residuals of ∼24 μs (see Fig. 2) and resulted in the parameters shown in Table 1.

4.1. *Cluster Accelerations*

It has been well established (e.g. Phinney 1992) that at least four different effects can contribute at the few percent or greater level to the measured spin-down rate, $\dot{P}$, of a MSP in a GC. Typically parameterized in terms of "accelerations," and ignoring the possible effects of a nearby star or planet perturbing the system, the measured acceleration of a pulsar is

$$\frac{\dot{P}}{P} = \frac{\dot{P}_o}{P} + \frac{a_{\ell,GC}}{c} + \frac{a_{\ell,Gal}}{c} + \frac{a_{PM}}{c}, \quad (1)$$

where $\dot{P}_o$ is the intrinsic spin-down of the pulsar, $a_{\ell,GC}/c$ and $a_{\ell,Gal}/c$ are the line-of-sight accelerations caused by the gravitational potentials of the cluster and the Galaxy, and $a_{PM}/c = \mu^2 D/c$ is the apparent acceleration caused by the transverse Doppler effect where μ is the pulsar's measured
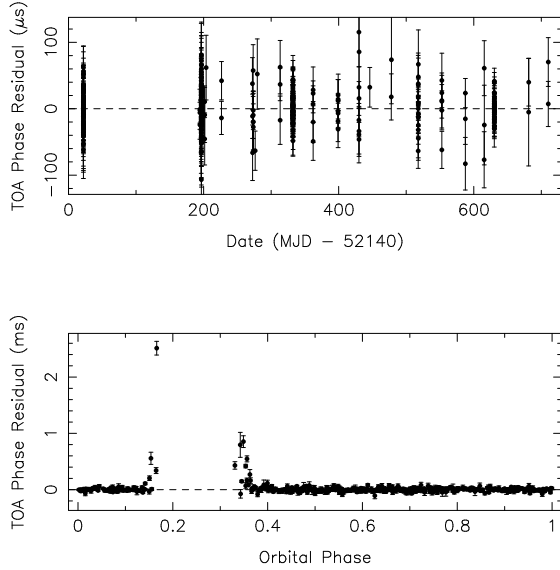
---
[11] http://pulsar.princeton.edu/tempo

FIG. 2.— (Top) Pulse phase residuals for pulsar M30A as determined after fitting for the timing model shown in Table 1 using TEMPO. All measured TOAs occurring between orbital phases 0.12–0.38 were excluded from the fit in order to minimize systematic effects caused by the pulse delays during eclipse ingress/egress. The RMS residual for the 408 TOAs is 23.7 μs. (Bottom) All measured phase residuals plotted as a function of orbital phase. For a circular orbit, eclipses are expected to occur during superior conjunction at a phase of 0.25. Eclipse delays of up to several ms are evident during eclipse ingress and egress (see §4.3).

TABLE 1. PARAMETERS FOR PSR J2140−2310A

Parameter	Value
Right Ascension, α (J2000)	$21^h\,40^m\,22\overset{s}{.}40610(46)$
Declination, δ (J2000)	$-23°\,10'\,48\overset{''}{.}7936(97)$
Dispersion Measure (pc cm^{-3})	25.0640(41)
Pulsar Period, P (ms)	11.0193290688805(67)
Period Derivative, $\dot{P}$ (s/s)	$-5.181(20)\times10^{-20}$
Epoch (MJD)	52162.0
Orbital Period, P_{orb} (days)	0.17398746418(34)
Projected Semi-Major Axis, x (lt-s)	0.2349416(48)
Eccentricity, e	$<1.2\times10^{-4}$
Epoch of Ascending Node, T_{ASC} (MJD)	52161.94552243(68)
Span of Timing Data (MJD)	52162–52850
Number of TOAs	408
Weighted RMS Timing Residual (μs)	23.7
Flux Density at 1400 MHz, S_{1400} (mJy)	0.08(3)

Derived Parameters	
Mass Function, f_1 (M$_\odot$)	0.000459967(28)
Minimum Companion Mass, m_2 (M$_\odot$)	≥ 0.10
Radio Luminosity, L_{1400} (mJy kpc^2)	6.5(2.5)

NOTE. — Numbers in parentheses represent the formal 2σ uncertainties in the last digit as determined by TEMPO, after scaling the TOA uncertainties such that $\chi^2_\nu/\nu = 1$. The values for f_1 and m_2 were derived assuming a pulsar mass of 1.4 M$_\odot$.

proper motion and D is its distance (Shklovskii 1970). Typically, the intrinsic spin-down and cluster acceleration terms are of the same order, while the Galactic and proper motion terms contribute at the 10% level or less.

In the case of M30 and M30A, we know that $\dot{P}/P = -4.7\times10^{-18}\,\text{s}^{-1}$ and can estimate $a_{\ell,\text{Gal}}/c \simeq -8.5\times10^{-19}\,\text{s}^{-1}$ assuming a spherically symmetric Galaxy with a flat rotation curve (Phinney 1993) and $a_{\text{PM}}/c \simeq 1.3\times10^{-18}\,\text{s}^{-1}$ given the 7.8 mas yr^{-1} of proper motion measured for M30

by Dinescu, Girard, & van Altena (1999). To an accuracy of $\sim10\%$, Phinney (1992, 1993) showed that

$$\max\frac{|a_{\ell,\text{GC}}|}{c} \simeq \frac{1.1G\overline{\Sigma}(<\Theta_\perp)}{c}, \qquad (2)$$

where $\overline{\Sigma}(<\Theta_\perp)$ is the projected surface mass density within the radial position of the pulsar in the cluster, $\Theta_\perp$ ($\sim3.6''$ for M30A). If the projected surface luminosity density is available from optical measurements, then we can use Equation 2 to place a lower limit to the projected mass-to-light ratio of the cluster within the radius of the pulsar position.

Using the power-law relation for the total-light V-band surface flux density in the core of M30 from Guhathakurta et al. (1998), we estimate the surface luminosity density within the radius of the position of M30A to be $\sim2.0\times10^4\,\text{L}_\odot\,\text{pc}^{-2}$. Substituting and rearranging Equation 1 implies that $M/L \gtrsim 0.51\,\text{M}_\odot/\text{L}_\odot$ in the core of M30, which is typical for GCs.

Phinney (1992, 1993) also showed that to within 10% if $\Theta_\perp < 2\Theta_c$,

$$\max\frac{|a_{\ell,\text{GC}}|}{c} \simeq \frac{3v_\ell^2(0)}{2cD\sqrt{\Theta_c^2+\Theta_\perp^2}}, \qquad (3)$$

where Θ_c is the core radius of the cluster (which we have assumed to be $\sim1.8''$ based on the range quoted by Yanny et al. 1994), and $v_\ell(0)$ is the one-dimensional velocity dispersion for the cluster core (9.4±2.5 km s^{-1} for M30 from Gebhardt et al. 1995). Since the measured $\dot{P}/P$ is negative, the intrinsic "acceleration" must be

$$\frac{\dot{P_o}}{P} < \max\frac{|a_{\ell,\text{GC}}|}{c} + \frac{\dot{P}}{P} - \frac{a_{\ell,\text{Gal}}}{c} - \frac{a_{\text{PM}}}{c}. \qquad (4)$$

If we account for the 1-σ error bars in D, $v_\ell(0)$, and the 10% accuracy of Equation 3, for M30A, $\dot{P_o}/P < 1.4\times10^{-16}\,\text{s}^{-1}$. Similarly, the surface magnetic field strength of M30A is $B_s = 3.2\times10^{19}(P\dot{P_o})^{1/2}\,\text{G} < 4.2\times10^9\,\text{G}$, the characteristic age $\tau_c = P/(2\dot{P_o}) > 1.1\times10^8\,\text{yr}$, and the spin-down luminosity $\dot{E} = 4\pi^2 I\dot{P_o}/P^3 < 4.6\times10^{34}\,\text{erg s}^{-1}$ assuming the canonical $I = 10^{45}\,\text{g cm}^2$. Each of these values is typical for MSPs.

4.2. Pulsed Flux

The monitoring observations have revealed significant diffractive scintillation (e.g. Rickett 1977) which results in large-scale variations of the measured flux density from M30A over time scales of one to several hours, and over bandwidths of 50–100 MHz. By integrating the pulsed signal above the average off-pulse levels and comparing the measured noise variance with that described by the radiometer equation, we have estimated the 20-cm flux density (S_{1400}) to an accuracy of $\sim30\%$ during 73 1-hour sub-integrations which occurred during un-eclipsed portions of the pulsar's orbit. We did not detect the pulsar during four of the sub-integrations, so for those epochs we assumed a flux density of 1/2 that of the weakest definite detection we have for the pulsar ($\sim16\,\mu$Jy), similar to the procedure used by Camilo et al. (2000). The measurements, displayed as a cumulative plot in Fig. 3, show the expected exponential distribution for strong diffractive scintillation (e.g. Rickett 1977) with an average flux density of $\sim0.08(3)$ mJy. We made similar measurements for 8 1-hour intervals at 575 MHz and 10 1-hour intervals at 820 MHz and found flux densities of approximately 0.13(4) mJy and 0.12(4) mJy respectively. These measurements correspond to a rather flat radio spectral index
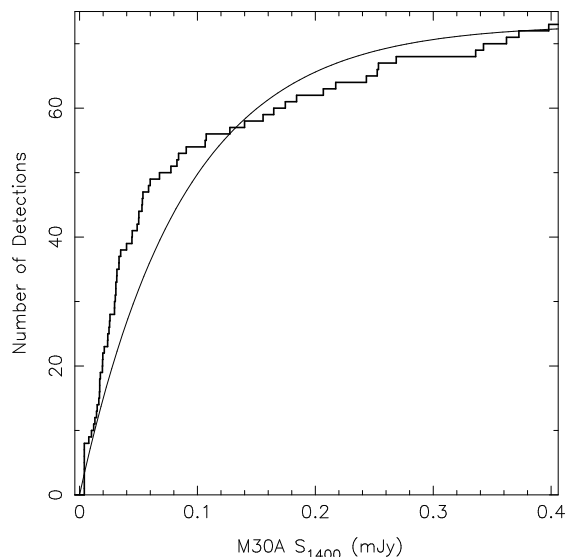
FIG. 3.— A cumulative plot of 73 measurements of the 20-cm flux density of pulsar M30A. Each measurement comprised an hour of integration time with the BCPM/GBT setup as described in §2. The thick curve shows a cumulative exponential distribution with an average of 87 μJy. The minimum detectable flux density in 1 hr was $\sim$16 μJy. During six of these 1-hr integrations that occurred outside of predicted eclipse times, the pulsar was undetected. For these points, we assumed a flux density of half the minimum detectable value, or 8 μJy.

for this pulsar of $-0.6^{+0.5}_{-0.7}$. With such a low average flux density, it is not surprising that M30A (and the less-luminous M30B; see §5) was not detected in earlier imaging surveys (Hamilton, Helfand, & Becker 1985, using the VLA) or pulsation searches (Biggs & Lyne 1996, using the 76-m Lovell Telescope at Jodrell Bank) of the cluster.

At the distance of M30, the 20-cm flux density for M30A corresponds to a radio luminosity $L_{1400} = 6.5(2.5)$ mJy kpc^2. Comparing this number to 40 MSPs in the most recent ATNF pulsar catalog (Manchester et al., in prep)[12] with measurements of L_{1400}, 11 catalog MSPs with measurements of L_{400} and assuming a typical spectral index for each of -1.6 (Lorimer et al. 1995), and the 14 MSPs in 47 Tucanae with estimates of L_{1400} in Camilo et al. (2000), we find that M30A is in the most luminous $\sim$30% of known MSPs, and more than twice as luminous as the median L_{1400} of $\sim$2.7 mJy kpc^2.

The lower frequency observations of M30A have revealed that the amplitude of the interpulse (as measured with respect to the main pulse) increases with decreasing radio frequency. While the separation in phase at each of the three observing bands 1400/820/575 MHz seems to be constant at $\sim$42%, the ratio of the flux contained in the main pulse to that in the interpulse is approximately 1.9/1.2/1.0 at 1400/820/575 MHz, respectively. Such frequency dependent evolution of pulse component amplitudes — while the pulse phases of the components remain constant — seems to be a common occurrence among pulsars (see e.g. Kramer et al. 1999, and references therein).

4.3. Eclipse Properties

M30A exhibits consistent and total eclipses at 1400, 820, and 575 MHz for approximately 20% of its orbital period centered on superior conjunction (i.e. orbital phase 0.25, see Figs. 1 and 2). The presence of eclipses implies that the orbit

[12] http://www.atnf.csiro.au/research/pulsar/psrcat/

is significantly inclined ($i > 30°$) and therefore the mass of the companion star is almost certainly in the range $0.10 \lesssim m_2 \lesssim 0.21$ M$_\odot$. As such, M30A ($P = 11.0$ ms, $P_{orb} = 0.174$ d) is very similar to the three other eclipsing MSPs with 0.1–0.25 M$_\odot$ companions and orbital periods of a few hours, all of which are located in GCs: PSR B1744−24A in Terzan 5 ($P = 11.6$ ms, $P_{orb} = 0.076$ d; Lyne et al. 1990), PSR J0024−7204W in 47 Tucanae ($P = 2.35$ ms, $P_{orb} = 0.133$ d; Camilo et al. 2000), and PSR J1701−3006B in M62 ($P = 3.59$ ms, $P_{orb} = 0.145$ d; Possenti et al. 2003).

Scintillation and pulse delays at eclipse ingress and egress (see below) make the determination of the exact duration of eclipses as a function of observing frequency difficult. From a single good 820 MHz observation, we measure the eclipse duration to be $0.23(2) P_{orb}$, while for four good observations near 1400 MHz, the eclipse duration is $0.18(1) P_{orb}$. This corresponds to a frequency dependence of the eclipse duration $\nu^{-\alpha}$ with $\alpha \sim 0.4$–0.5, very similar to that measured by Fruchter et al. (1990) for PSR B1957+20. Such a value is also consistent with the cyclotron absorption based eclipse model of Khechinashvili, Melikidze, & Gil (2000), where the absorption occurs in the magnetosphere of the degenerate companion star which gets continuously injected with relativistic particles from the pulsar wind.

During times of increased signal-to-noise ratio due to scintillation, we observe pulse phase delays of up to 2−3 ms during eclipse ingress and egress which imply the presence of an additional electron column density of $N_e \sim 7.4 \times 10^{17} \Delta_{t,ms} \nu_{GHz}^2$ cm^{-2} in the eclipse region, where $\Delta_{t,ms}$ is the pulse delay in ms, and ν_{GHz} is the observing frequency in GHz (see Fig. 2). For our observations of M30A, this corresponds to $N_e \gtrsim 2 \times 10^{18}$ cm^{-2}. Since the orbital separation of the system is $a \sim 1.4$ R$_\odot$ (for $i \gtrsim 60°$) an eclipse duration of $\sim$20% of the orbital period corresponds to a physical size of the eclipsing region R_E of $\sim$0.9 R$_\odot$. The additional electron density near the eclipse boundaries is therefore $\gtrsim 3 \times 10^7$ cm^{-3} which corresponds to a plasma density of $\rho_E \gtrsim 5 \times 10^{-17}$ g cm^{-3} if fully ionized.

As in the cases of the other eclipsing MSPs with low-mass companions, the physical sizes of plausible companion types is much smaller than R_E. Assuming $i = 60°$ and therefore $m_{2,60°} = 0.12$ M$_\odot$, hydrogen and helium white dwarfs (WDs) have radii of $\sim$0.08 R$_\odot$ or $\sim$0.03 R$_\odot$ respectively (Shapiro & Teukolsky 1983), while a zero-age main sequence star would have a radius of $\sim$0.13 R$_\odot$. Even the Roche lobe radius $R_L \sim 0.26$ R$_\odot$ (e.g. Eggleton 1983) is several times smaller than R_E, implying that the eclipses must be due to wind- or magnetosphere-related activity at several times the companion radius (Fruchter et al. 1990; Stappers et al. 1996; Khechinashvili et al. 2000). If this wind is emitted isotropically, the plasma density at the eclipse boundaries corresponds to a mass loss rate $\dot{M} = 4\pi R_E^2 \rho_E v_w$, where v_w is the velocity of the ionized wind from the companion. If we assume $v_w \sim 10^8$ cm s^{-1}, which is the order of the escape velocity from the surface of a presumed WD companion, the corresponding mass loss rate is $\dot{M} \sim 4 \times 10^{-12}$ M$_\odot$ yr^{-1}. As has been found with the other eclipsing systems, unless the ionized fraction of the eclipsing wind is small ($\lesssim 0.4$), the companion star will not be ablated in a Hubble time.

The nature of the eclipse mechanism for M30A is currently difficult to constrain given that we know neither the true spin-down luminosity of the pulsar nor the nature of the companion star. Additionally, the low average flux density of M30A has

allowed only a few good measurements of the eclipse ingress and egress. However, it does seem unlikely that the eclipses are caused by dispersive smearing of the pulses, since the excess N_e that we measure near the eclipse boundaries would cause $\lesssim 1$ ms of smearing across the bandwidth of our observations and would therefore not smear the pulse enough for it to appear eclipsed. While our initial measurement of the frequency dependence of the eclipse duration seems to be in reasonable agreement with the cyclotron absorption model of Khechinashvili et al. (2000), better constraints on the eclipse mechanism will have to await higher sensitivity observations as well as good measurements of the eclipse properties at several other observing frequencies.

4.4. *Optical Observations*

We have attempted to identify the companion of M30A in archival *HST*/WFPC2 observations of M30. We have used the observations in the F336W, F439W and F555W filters (hereafter U_{336}, B_{439} and V_{555}) of GO-5324 (1994 March 1) and the observations in the U_{336}, V_{555} and F814W (hereafter I_{814}) filters of GO-7379 (1999 May 31 and June 1). The exposure times of these observations are 200 s in U_{336}, 80 s in B_{439} and 16 s in V_{555} for the GO-5324 program and 11 600 s in U_{336}, 1192 s in V_{555} and 1676 s in I_{814} for GO-7379. These images were reduced and photometered with the HSTphot 1.1 package by Dolphin (2000), following the recommended procedures in the HSTphot manual[13].

The *HST*/WFPC2 images were placed onto the International Celestial Reference System (ICRS) for direct comparison against the position of the pulsar (Table 1). A detailed description of this procedure is presented in Bassa et al. (2003). In short, a $8' \times 8'$ section of a 4 minute V-band image, taken 2000 August 28 with the Wide Field Imager (WFI) at the ESO 2.2 m telescope at La Silla, was placed onto the ICRS using 58 stars from the USNO CCD Astrograph Catalog (UCAC; Zacharias et al. 2000). We fitted for zero-point position, scale and position angle, and the astrometric solution has rms residuals of $0.06''$ in both right ascension and declination. This solution was transferred to the WFPC2 images by matching stars on the WFI with those on the WFPC2 chips, where we corrected the WFPC2 pixel positions for geometric distortion and placed them on a master frame following the prescription of Anderson & King (2003). A total of 99 stars were used for the GO-7379 dataset (105 for GO-5324), giving rms residuals of $0.05''$ to $0.06''$ in both coordinates. The final (1σ) uncertainty in the astrometric solution of the WFPC2 images is about $0.07''$ to $0.08''$ in right ascension and declination. A $4'' \times 4''$ section of an image comprising 1044 s of the V_{555} data from GO-7379 is shown in Figure 4. The image shows a single star within the $0.25''$ (95% confidence) error circle centered on the M30A position. The star is offset from the pulsar position by $-0.09''$ in right ascension and $-0.07''$ in declination and is a plausible companion to M30A.

HSTphot identified and measured the magnitude of the candidate companion to M30A in 13 of the 48 individual V_{555} images from GO-7379, but failed to detect it in the U_{336} and I_{814} images. The S/N ratio of the V_{555} detections is very low, roughly between 2–5, and hence the uncertainties in the magnitude determinations are large (typically 0.4 magnitudes). The average V_{555} magnitude of the candidate from the 13 detections is 23.8 ± 0.1. We folded the magnitude measurements at the orbital period of the pulsar using the ephemeris
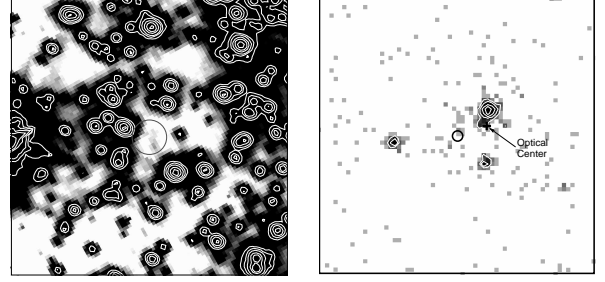
FIG. 4.— Optical V_{555}-band (left) and X-ray (right) images of portions of M30. North is towards the top in each image and east to the left. (Left) A $4'' \times 4''$ *HST*/WFPC2 F555W (V_{555}) image with a total exposure of 1044 s centered on the radio position of M30A. The error circle has a radius of $0.25''$ and is the 95% confidence region for the position of M30A in the optical frame. A single star is present in the error circle, right and below of the center. The countour levels correspond to 50, 100, 200, 500, 1000, and 2000 counts. See §4.4 for more details. (Right) A 50 ks, $32'' \times 32''$ *Chandra* ACIS-S3 0.2–3 keV image of the central portion of M30. Light grey pixels indicate a single detected photon, while darker pixels indicate two or more counts. Contour levels correspond to 5, 15, 50, and 150 counts. The error circle has a radius of $0.6''$ which is the approximate error in the absolute astrometry of the *Chandra* image. The astrometrically corrected position of the optical center of the cluster as determined by Guhathakurta et al. (1998) is marked with a black cross. We consider it likely that the ~5 events just to the northwest of the nominal pulsar position are from M30A. See §4.5 for more details.

in Table 1 but found no significant variability, possibly due to the large uncertainties in the magnitudes. We note that the non-detections occur roughly uniformly in orbital phase and therefore cannot be explained exclusively by orbital phase dependent variability. These measurements are consistent with visual inspection of the candidate position on the individual V_{555} images. The non-detections of the candidate companion in U_{336} and I_{814} place the object on or bluewards of the cluster main sequence.

Whether or not this candidate is the actual companion to M30A, it is unlikely that the true companion is similar to that of PSR J1740−5340A in NGC 6397 (Ferraro et al. 2001). That star is as luminous as stars at the main sequence turn off, while the U_{336} magnitude of the candidate companion to M30A is at least 5 magnitudes fainter than that. If the companion is a main sequence star, it is more likely comparable to PSR J0024−7204W in 47 Tucanae (Camilo et al. 2000), whose binary companion was recently identified in *HST* observations on the basis of large-amplitude variability which matched the orbital period and phase of the pulsar (Edmonds et al. 2002). Since M30A has similar orbital characteristics to 47 Tuc W, it is plausible that the companion to M30A shows optical variability as well. The current V_{555} data, though, rule out variability at the 1.6 mag level as seen from 47 Tuc W. A future series of *HST*/ACS images might unambiguously identify our candidate as the companion to M30A on the basis of lower amplitude variability or detect a more likely counterpart.

We have followed the recommendation of Guhathakurta et al. (1998) and matched their astrometry against our astrometric solution of the GO-5324 dataset. We find that their reference star (No. 3611) has an absolute position of $\alpha_{2000} = 21^h 40^m 22\overset{s}{.}314$ and $\delta_{2000} = -23° 10' 40\overset{''}{.}10$. We have furthermore matched the Guhathakurta et al. (1998) positions of the 40 stars in their Table 1 against our positions and solved for zero-point offset, scale and rotation. The Guhathakurta et al. (1998) frame had to be shifted by $-1.25''$ and $2.27''$ in R.A. and in Decl., scaled by a factor of 0.988

in both axes and rotated by $-0.76°$ around the new position of the reference star, to result in our astrometric frame. The rms residuals of the transformation were about $0.006''$ in both coordinates. In our absolute astrometric frame the Guhathakurta et al. (1998) position of the M30 centroid has $\alpha_{2000} = 21^{\rm h} 40^{\rm m} 22\fs16$ and $\delta_{2000} = -23° 10' 47\farcs6$. We use this position for the M30 cluster center throughout the paper.

4.5. X-ray Observations

We have also attempted to identify pulsar M30A in a 50 ks *Chandra* ACIS-S3 observation centered on the core of M30 and taken 2001 November 19 (OBSID 2679). We used the CIAO[14] software package (v3.01 with CALDB v2.23) to apply the most up-to-date aspect, charge transfer inefficiency, and gain map corrections to produce a new Level=2 events file from the archival Level=1 events. From that file we kept all events with energies in the range $0.3-3$ keV in order to produce the $32'' \times 32''$ image of the cluster core shown in Figure 4. Just to the north-west of the nominal pulsar position there appears to be a weak (~5 counts with energy <3 keV) source. While this "source" was not detected by the WAVDETECT algorithm, given that several eclipsing MSPs have been identified in X-rays (e.g. Grindlay et al. 2002; Stappers et al. 2003), and that the timing position of M30A is within the $\sim0\farcs6$ absolute astrometric error circle for *Chandra*, it is plausible that the observed X-ray flux originates from M30A.

If we assume a blackbody model (using PIMMS[15]) with a single $kT \sim 0.22$ keV (as in Grindlay et al. 2002) and a N_H for M30 of 3.5×10^{20} cm^{-2} (Dickey & Lockman 1990), the five measured events in the $0.3-3$ keV band correspond to an equivalent unabsorbed flux from the source of $\sim 5 \times 10^{-16}$ ergs cm^{-2} s^{-1}, which at the distance of M30 corresponds to a luminosity of $\sim 5 \times 10^{30}$ ergs s^{-1}. This is comparable to the X-ray luminosities found for the MSPs in 47 Tucanae and NGC 6397 which are believed to be due to emission from hot polar caps on the NSs (Grindlay et al. 2002). Alternatively, the emission could be due to thermal bremsstrahlung (TB) in the hot ionized wind of the companion star where the radio eclipses take place. While a TB model with $T \sim 1$ keV yields an almost identical luminosity of $\sim 6 \times 10^{30}$ ergs s^{-1}, the implied emission measure would be EM $\sim 2 \times 10^{54}$ cm^{-3}. If we assume the plasma to be fully ionized and uniformly distributed in a spherical region of diameter R_E, the total volume of the plasma is $\sim 1.3 \times 10^{32}$ cm^3 and the corresponding electron density is $\sim 1 \times 10^{11}$ cm^{-3}. This value is ~ 3000 times larger than the measured electron density near the eclipse boundaries (§4.3). Since the eclipsing material is being constantly replenished (based on the fact that size of the eclipsing region is much larger than even the Roche lobe radius of the companion) and since we measure no dispersive delays outside of the orbital phases corresponding to the eclipse region, the very large electron densities implied by TB effectively rule it out as the source of the X-ray emission. An additional argument against the TB model comes from the fact that the isolated MSPs in 47 Tucanae show X-ray emission yet have no companion stars to generate the required hot ionized wind.

5. PULSAR J2140−23B (M30B)

For each of the timing observations, we searched the data using the same techniques described in §2 both for new pulsars and for a re-appearance of M30B. In addition, we performed limited folding searches of 20-min to 1-hr data segments for M30B over a range of periods centered on its discovery spin period and a range of plausible period derivatives that would be caused by the accelerations of the possible orbits discussed in §5.1. In no case have we either definitively re-detected M30B or confirmed any additional pulsars in the cluster.

Our lack of subsequent detections of pulsar M30B can be explained in one of two ways. The most likely explanation is simply that M30B has a significantly lower average flux density than M30A, and that its discovery was the result of an extreme diffractive scintillation event. Given the exponential distribution of diffractive scintillation events, however, and the implied low probability of observing extreme scintillation events, it is unlikely that M30B has a flux density more than a factor of ~2 below that of M30A. This implies that if diffractive scintillation is the cause for our non-detections in blind searches, then the pulsar would be visible in much of our data if we could search for it optimally (i.e. folding on the correct orbital ephemeris). We note that M30A is not detectable via blind searches in approximately half of our observations.

The other possibility for the non-detections of M30B is unusual eclipses. It could be that M30B has an intrinsic luminosity similar to or even greater than that of M30A, but its companion causes irregular and possibly long-term "eclipses" of the pulsed signal in the same manner as the GC MSPs PSR B1744−24A in Terzan 5 (Lyne et al. 1990; Nice & Thorsett 1992) and PSR J1740−5340 in NGC 6397 (D'Amico et al. 2001b).

5.1. Orbit Constraints

Without post-discovery detections of M30B we are currently unable to unambiguously determine the orbital parameters of the system. However, examination of the spin-frequency behavior during the more than seven hours that the pulsar was visible in the 2001 September 9 discovery observation immediately led us to conclude that we could not fit a sinusoid to the frequency behavior (see Fig. 5), and hence that the orbit was significantly eccentric.

We measured 26 TOAs from the BCPM1 and BCPM2 discovery observations and used TEMPO to fit a timing model consisting of the DM of M30B and a Taylor expansion of the measured pulsation frequency in time. Reasonable solu-
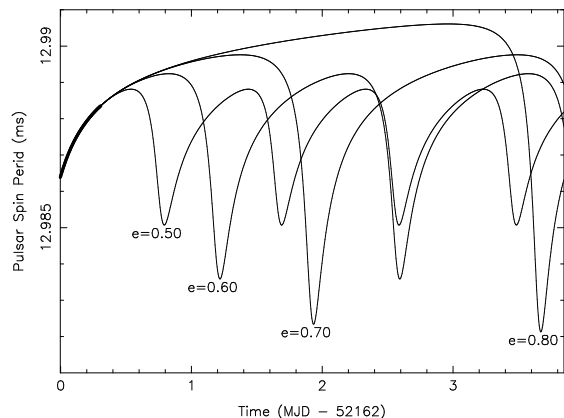
FIG. 5.— The predicted time dependence of the measured spin period of M30B given four representative Keplerian orbital solutions from the family shown in Fig. 6. The thick black line shows the measured spin period during the discovery observations of 2001 September 9.

tions providing "white" timing residuals required fits to the initial spin frequency (f) and at least the first four frequency derivatives ($\dot{f}$, $\ddot{f}$, $f^{(3)}$, and $f^{(4)}$). The best 4-derivative solution, at an MJD(UTC) epoch of 52161.997395, and a DM of $25.09\pm0.12\,\mathrm{pc\,cm^{-3}}$, is

$$f = 77.003746(14)\,\mathrm{Hz},$$
$$\dot{f} = -8.557(59) \times 10^{-7}\,\mathrm{Hz\,s^{-1}},$$
$$\ddot{f} = 5.68(16) \times 10^{-11}\,\mathrm{Hz\,s^{-2}},$$
$$f^{(3)} = -4.06(25) \times 10^{-15}\,\mathrm{Hz\,s^{-3}},$$
$$f^{(4)} = 1.79(19) \times 10^{-19}\,\mathrm{Hz\,s^{-4}},$$

and provided RMS residuals of $\sim 53\,\mu$s and the pulse profile shown in Fig. 1.

Given the timing solution above, we applied the orbit-inversion technique described by Joshi & Rasio (1997) to convert the polynomial-based solution into a family of Keplerian orbital solutions as a function of orbital eccentricity, e (assuming that the intrinsic $\dot{f}$ for the pulsar is negligible during the observation). A lack of physical solutions from the technique provided a rough lower limit to M30B's eccentricity of $e \gtrsim 0.45$. Using the inversion-based family of solutions as starting points at a series of trial eccentricities, and setting the DM to the value measured earlier, we used TEMPO to compute χ^2_ν surfaces (with $\nu=22$ degrees-of-freedom) as a function of P_{orb} and x, by allowing the software to fit for f, the angle of periastron (ω) and the time since periastron (T_0). The values of P_{orb} and x at the resulting χ^2_ν minima are plotted in Fig. 6, and have typical errors in each parameter of 10–20%. This process provided a 95% confidence lower limit to the eccentricity of $e \geq 0.52$. Orbits with $e \geq 0.55$ provided essentially perfect fits to the data with $\chi^2_\nu/\nu \sim 1.0$ and white-noise-like residuals with an RMS of $\sim 30\,\mu$s. The spin-period behavior of four representative orbital solutions is plotted in Fig. 5 as well as the measured spin-period behavior during the discovery observation.

The family of orbital solutions that we have determined implies that M30B is part of a relativistic orbital system with a companion most likely in the mass range 0.25–1 $M_\odot$. If the companion is a white dwarf (WD), the advance of periastron ($\dot{\omega}$) due to general relativity will be several tenths of a degree per year and would be measurable (as will, therefore, the total system mass, $M = m_1 + m_2$) to a high degree of precision within a year of monthly timing observations of a quality similar to the discovery observation. It is also possible, if such timing measurements can be made on a consistent basis, that additional post-Keplerian orbital parameters, such as the Einstein γ, will be measurable in M30B within several years. Such measurements would provide one of the few accurate mass determinations of a MSP which is important for testing models of NS spin-up via accretion. Most models predict the accumulation of $\gtrsim 0.1\,M_\odot$ of material onto the NS during the spin-up process (Phinney & Kulkarni 1994, and references therein), and recent observations have begun providing evidence for the case (e.g. Nice, Splaver, & Stairs 2003).

In the current pulsar catalog, there are only four other GC binary pulsars with $e > 0.1$. The NS–NS system in M15, PSR B2127−11C ($P = 30.5$ ms, $P_{orb} = 0.335$ d, $e = 0.681$; Prince et al. 1991) was almost certainly created in an exchange interaction near the core of the cluster that replaced a lower-mass MS or WD companion of a NS with another NS (Phinney & Sigurdsson 1991; Sigurdsson & Phinney 1993). This interaction also placed the system as a whole in a highly
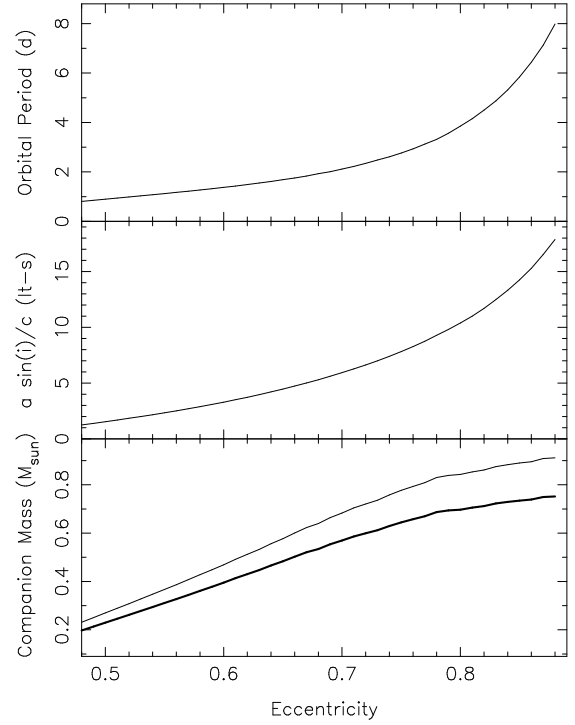

FIG. 6.— The family of possible Keplerian orbital solutions for M30B based on TEMPO fits to 26 TOAs determined during the discovery observation. The 95% confidence lower-limit to the eccentricity is $e \gtrsim 0.52$ (see §5.1). For P_{orb} (top) and $a\sin(i)/c$ (middle), typical uncertainties are 10–20% in the plotted value. In the bottom panel, the lower line shows the minimum companion mass ($i = 90°$) while the upper line represents the mass corresponding to the median inclination, $i = 60°$, assuming random inclinations. In all cases we have assumed a pulsar mass of $m_1 = 1.4\,M_\odot$.

eccentric orbit around the center-of-mass of M15, which explains its location near the outskirts of the cluster today. An exchange interaction also provides the most likely explanation for the eccentricity of PSR B1802−07 in NGC 6539 ($P = 23.1$ ms, $P_{orb} = 2.62$ d, $e = 0.212$; D'Amico et al. 1993) — a system possibly very similar to M30B — and a possible explanation for the eccentricity of PSR B1516+02B in M5 ($P = 7.95$ ms, $P_{orb} = 6.86$ d, $e = 0.138$; Anderson et al. 1997) as well. Rasio & Heggie (1995) have argued, however, that M5B's eccentricity may be the product of many distant interactions with other stars near the clusters core over several Gyr. The fourth cluster binary pulsar with a large eccentricity is the recently discovered PSR J1750−37 in NGC 6441 ($P = 111.6$ ms, $P_{orb} = 17.3$ d, $e = 0.71$; Possenti et al. 2001), which may be a very similar system to M30B, albeit with a much slower spin period. Hypotheses of its origin await determination of its position with respect to the cluster center, but with such a large eccentricity, an exchange encounter seems likely.

We can estimate the time required for a pulsar with an initially near-circular orbit in the core of M30 to accumulate an eccentricity of $e \geq 0.5$ by using Equation 5 from Rasio & Heggie (1995). With a one-dimensional velocity dispersion for the cluster core of $v_\ell(0)=9.4\pm2.5\,\mathrm{km\,s^{-1}}$ (Gebhardt et al. 1995), and the number density of stars in the core of $\sim 1.6 \times 10^5\,\mathrm{pc^{-3}}$ (Guhathakurta et al. 1998), we estimate $t_{e\geq0.5} \simeq 7P_{orb,d}^{-2/3}$ Gyr, where $P_{orb,d}$ is the orbital period of M30B in days. Therefore, if M30B resides in the core of M30, it is possible that its eccentricity is due to many distant interac-

tions. It is interesting to note that for M30A, which probably does reside in the core of M30, the time required for multiple distant interactions to produce an eccentricity that would be detectable in our current measurements ($e \sim 2 \times 10^{-4}$) is $\sim$2–3 Gyr. This means that M30A is either younger than $\sim$2–3 Gyr, or the mechanism described by Rasio & Heggie (1995) is not as efficient in M30 as we calculate.

Should M30B reside outside of the cluster core, that may indicate that its high eccentricity was caused by an exchange interaction similar to that which could have produced PSR B1802−07 and almost certainly did produce the recently discovered eclipsing MSP in the outskirts of NGC 6397, PSR J1740−5340 (D'Amico et al. 2001b). If the exchange interaction replaced a low-mass WD with a MS star, optical observations should allow its identification, once a timing position has been measured. Such a MS or even post-MS companion could help to explain our lack of detections of the pulsar as well. If the companion star experiences significant though possibly erratic mass loss, the pulsed flux from M30B could be eclipsed or even quenched entirely for periods at a time, just as observed from PSR J1740−5340. If this is the case, higher frequency observations of the cluster may allow us to peer through the wind of the companion and see the pulsar consistently.

If the companion to M30B is a MS or post-MS star, though, orbital circularization due to a hydrodynamical mechanism (Tassoul 1995) may occur on timescales much shorter than the $\sim 10^{8-10}$ yr age of the system we would expect if it was created via an exchange interaction. Tassoul (1995) calibrated a theoretical relation for hydrodynamical orbit circularization by comparing the shortest orbital periods of MS binaries with eccentric orbits in several stellar clusters of different ages. He determined the time for circularization in years to be roughly $t_{circ} \sim 1.5 \times 10^{(7-N/4)} P_{orb,d}^{49/12}$, where the fitting paramer $N \sim 8.3$ for stellar systems of age >1 Gyr and $P_{orb,d}$ is the orbital period in days. For the family of orbital solutions we have found for M30B, this corresponds to $t_{circ} \sim 10^{5-9}$ yr, and implies either that the companion star is a WD, or that the interaction that exchanged a MS companion into the system happened within the last 10^9 yrs, or significantly more recently if the orbital period of M30B is $\lesssim$6 d. We note, though, that the Tassoul (1995) calculations assume a binary system of two MS stars and almost certainly need modification for NS−MS systems.

6. CONCLUSIONS

We have used the Green Bank Telescope to discover two binary MSPs in the core-collapsed GC M30. One of these systems is a member of the rapidly growing class of eclipsing MSPs and the other seems to be in a highly eccentric and relativistic orbit. Higher sensitivity observations of M30 in the near future — for instance, using all of the available bandwidth provided by the GBT's 20-cm receiver — should allow us to monitor M30A for long-term variations in its orbital parameters as has been seen in other eclipsing MSPs (e.g. Arzoumanian, Fruchter, & Taylor 1994) and enable us to consistently detect and time M30B. Additional observations at other radio frequencies will allow us to probe the eclipse region of M30A to a greater degree, and will hopefully allow us to constrain the mechanism behind the eclipses themselves.

It seems clear that as in the case of most other GCs (e.g. Camilo et al. 2000), we are only seeing the most luminous pulsars contained in M30. Given the extreme scintillation events we have witnessed from M30A and B, we consider it quite likely that the improved observations mentioned above will uncover several additional pulsars in M30 in the years ahead.

REFERENCES

Anderson, J. & King, I. R. 2003, PASP, 115, 113

Anderson, S. B., Wolszczan, A., Kulkarni, S. R., & Prince, T. A. 1997, ApJ, 482, 870

Arzoumanian, Z., Fruchter, A. S., & Taylor, J. H. 1994, ApJ, 426, L85

Backer, D. C., Dexter, M. R., Zepka, A., Ng, D., Werthimer, D. J., Ray, P. S., & Foster, R. S. 1997, PASP, 109, 61

Bassa, C. G., Verbunt, F., van Kerkwijk, M. H., & Homer, L. 2003, A&A, 409, L31

Biggs, J. D. & Lyne, A. G. 1996, MNRAS, 282, 691

Camilo, F., Lorimer, D. R., Freire, P., Lyne, A. G., & Manchester, R. N. 2000, ApJ, 535, 975

Carretta, E., Gratton, R. G., Clementini, G., & Fusi Pecci, F. 2000, ApJ, 533, 215

Chandler, A. M. 2003, PhD thesis, California Institute of Technology

Cordes, J. M. & Lazio, T. J. W. 2002, astro-ph/0207156

D'Amico, N., Bailes, M., Lyne, A. G., Manchester, R. N., Johnston, S., Fruchter, A. S., & Goss, W. M. 1993, MNRAS, 260, L7

D'Amico, N., Lyne, A. G., Manchester, R. N., Possenti, A., & Camilo, F. 2001a, ApJ, 548, L171

D'Amico, N., Possenti, A., Fici, L., Manchester, R. N., Lyne, A. G., Camilo, F., & Sarkissian, J. 2002, ApJ, 570, L89

D'Amico, N., Possenti, A., Manchester, R. N., Sarkissian, J., Lyne, A. G., & Camilo, F. 2001b, ApJ, 561, L89

Dickey, J. M. & Lockman, F. J. 1990, ARA&A, 28, 215

Dinescu, D. I., Girard, T. M., & van Altena, W. F. 1999, AJ, 117, 1792

Dolphin, A. E. 2000, PASP, 112, 1383

Edmonds, P. D., Gilliland, R. L., Camilo, F., Heinke, C. O., & Grindlay, J. E. 2002, ApJ, 579, 741

Eggleton, P. P. 1983, ApJ, 268, 368

Ferraro, F. R., Possenti, A., D'Amico, N., & Sabbi, E. 2001, ApJ, 561, L93

Freire, P. C., Camilo, F., Kramer, M., Lorimer, D. R., Lyne, A. G., Manchester, R. N., & D'Amico, N. 2003, MNRAS, 340, 1359

Freire, P. C., Camilo, F., Lorimer, D. R., Lyne, A. G., Manchester, R. N., & D'Amico, N. 2001a, MNRAS, 326, 901

Freire, P. C., Kramer, M., Lyne, A. G., Camilo, F., Manchester, R. N., & D'Amico, N. 2001b, ApJ, 557, L105

Fruchter, A. S., Berman, G., Bower, G., Convery, M., Goss, W. M., Hankins, T. H., Klein, J. R., Nice, D. J., Ryba, M. F., Stinebring, D. R., Taylor, J. H., Thorsett, S. E., & Weisberg, J. M. 1990, ApJ, 351, 642

Gebhardt, K., Pryor, C., Williams, T. B., & Hesser, J. E. 1995, AJ, 110, 1699

Grindlay, J. E., Camilo, F., Heinke, C., Edmonds, P. D., Cohn, H., & Luger, P. 2002, ApJ, 581, 470

Guhathakurta, P., Webster, Z. T., Yanny, B., Schneider, D. P., & Bahcall, J. N. 1998, AJ, 116, 1757

Hamilton, T. T., Helfand, D. J., & Becker, R. H. 1985, AJ, 90, 606

Jacoby, B. A., Chandler, A. M., Backer, D. C., Anderson, S. B., Kulkarni, S. R., & Green, D. W. E. 2002, IAU Circ., 7783, 1

Johnston, H. M. & Kulkarni, S. R. 1991, ApJ, 368, 504

Joshi, K. J. & Rasio, F. A. 1997, ApJ, 479, 948, (Errata: 488, 901)

Khechinashvili, D. G., Melikidze, G. I., & Gil, J. A. 2000, ApJ, 541, 335

Kramer, M., Lange, C., Lorimer, D. R., Backer, D. C., Xilouris, K. M., Jessner, A., & Wielebinski, R. 1999, ApJ, 526, 324

Kulkarni, S. R. & Anderson, S. B. 1996, in Dynamical Evolution of Star Clusters – Confrontation of Theory and Observations: IAU Symposium 174, Vol. 174, 181

Lorimer, D. R., Camilo, F., Freire, F., Kramer, M., Lyne, A. G., Manchester, R. N., & D'Amico, N. 2003, in ASP Conf. Series 302: Radio Pulsars, ed. M. Bailes, D. Nice, & S. Thorsett, 363

Lorimer, D. R., Yates, J. A., Lyne, A. G., & Gould, D. M. 1995, MNRAS, 273, 411

Lyne, A. G., Johnston, S., Manchester, R. N., Staveley-Smith, L., & D'Amico, N. 1990, Nature, 347, 650

Nice, D. J., Splaver, E. M., & Stairs, I. H. 2003, in ASP Conf. Series 302: Radio Pulsars, ed. M. Bailes, D. Nice, & S. Thorsett, 75

Nice, D. J. & Thorsett, S. E. 1992, ApJ, 397, 249

Phinney, E. S. 1992, Phil. Trans. Roy. Soc. A, 341, 39

Phinney, E. S. 1993, in ASP Conf. Series 50: Structure and Dynamics of Globular Clusters, ed. S. Djorgovski & G. Meylan, 141

Phinney, E. S. & Kulkarni, S. R. 1994, ARA&A, 32, 591

Phinney, E. S. & Sigurdsson, S. 1991, Nature, 349, 220

Possenti, A., D'Amico, N., Manchester, R. N., Camilo, F., Lyne, A. G., Sarkissian, J., & Corongiu, A. 2003, ApJ, in press (astro-ph/0308372)

Possenti, A., D'Amico, N., Manchester, R. N., Sarkissian, J., Lyne, A. G., & Camilo, F. 2001, astro-ph/0108343

Prince, T. A., Anderson, S. B., Kulkarni, S. R., & Wolszczan, W. 1991, ApJ, 374, L41

Ransom, S. M. 2001, PhD thesis, Harvard University

Ransom, S. M., Cordes, J. M., & Eikenberry, S. S. 2003, ApJ, 589, 911

Ransom, S. M., Eikenberry, S. S., & Middleditch, J. 2002, AJ, 124, 1788

Rasio, F. A. & Heggie, D. C. 1995, ApJ, 445, L133

Rickett, B. J. 1977, ARA&A, 15, 479

Shapiro, S. L. & Teukolsky, S. A. 1983, Black Holes, White Dwarfs and Neutron Stars. The Physics of Compact Objects (New York: Wiley–Interscience)

Shklovskii, I. S. 1970, Soviet Ast., 13, 562

Sigurdsson, S. 2003, in ASP Conf. Series 302: Radio Pulsars, ed. M. Bailes, D. Nice, & S. Thorsett, 391

Sigurdsson, S. & Phinney, E. S. 1993, ApJ, 415, 631

Standish, E. M. 1982, A&A, 114, 297

Stappers, B., Gaensler, B., Kaspi, V., van der Klis, M., & Lewin, W. 2003, Science, 299, 1372

Stappers, B. W., Bailes, M., Lyne, A. G., Manchester, R. N., D'Amico, N., Tauris, T. M., Lorimer, D. R., Johnston, S., & Sandhu, J. S. 1996, ApJ, 465, L119

Staveley-Smith, L., Wilson, W. E., Bird, T. S., Disney, M. J., Ekers, R. D., Freeman, K. C., Haynes, R. F., Sinclair, M. W., Vaile, R. A., Webster, R. L., & Wright, A. E. 1996, Proc. Astron. Soc. Aust., 13, 243

Tassoul, J. 1995, ApJ, 444, 338

Taylor, J. H. 1992, Phil. Trans. Roy. Soc. A, 341, 117

Taylor, J. H. & Cordes, J. M. 1993, ApJ, 411, 674

Yanny, B., Guhathakurta, P., Schneider, D. P., & Bahcall, J. N. 1994, ApJ, 435, L59

Zacharias, N., Urban, S. E., Zacharias, M. I., Hall, D. M., Wycoff, G. L., Rafferty, T. J., Germain, M. E., Holdenried, E. R., Pohlman, J. W., Gauss, F. S., Monet, D. G., & Winter, L. 2000, AJ, 120, 2131